Improvement of vertical profiles of raindrop size distribution from micro rain radar using 2D video disdrometer measurements

E. Adirosi(1,2), L. Baldini(1), N. Roberto(1), P. Gatlin(3), A. Tokay (4)

(1) CNR – Istituto di Scienze dell'Atmosfera e del Clima, Roma, Italy
(2) Dipartimento di Ingegneria Civile, Edile e Ambientale, Sapienza Università di Roma, Rome, Italy
(3) NASA Marshall Space Flight Center, Huntsville, Alabama
(4) NASA Goddard Space Flight Center, Greenbelt, MD, and University of Maryland, Baltimore County, Baltimore, MD

Elisa Adirosi
Consiglio Nazionale delle Ricerche
Istituto di Scienze dell'Atmosfera e del Clima
Via Fosso del Cavaliere, 100 - 00133 Roma, Italy
Tel: +39 06 49934325

Postprint of: E. Adirosi, L. Baldini, N. Roberto, P. Gatlin, A. Tokay, Improvement of vertical profiles of raindrop size distribution from micro rain radar using 2D video disdrometer measurements, Atmospheric Research, Volume 169, Part B, 2016, Pages 404-415.
https://doi.org/10.1016/j.atmosres.2015.07.002.

Abstract

A measurement scheme aimed at investigating precipitation properties based on collocated disdrometer and profiling instruments is used in many experimental campaigns. Raindrop size distribution (RSD) estimated by disdrometer is referred to the ground level; the collocated profiling instrument is supposed to provide complementary estimation at different heights of the precipitation column above the instruments. As part of the Special Observation Period 1 of the HyMeX (Hydrological Cycle in the Mediterranean Experiment) project, conducted between 5 September and 6 November 2012, a K-band vertically pointing micro rain radar (MRR) and a 2D video disdrometer (2DVD) were installed close to each other at a site in the historic center of Rome (Italy). The raindrop size distributions collected by 2D video disdrometer are considered to be fairly accurate within the typical sizes of drops. Vertical profiles of raindrop sizes up to 1085 meters are estimated from the Doppler spectra measured by the micro rain radar with a height resolution of 35 meters. Several issues related to vertical winds, attenuation correction, Doppler spectra aliasing, and range-Doppler ambiguity limit the performance of MRR in heavy precipitation or in convection, conditions that frequently occur in late summer or in autumn in Mediterranean regions. In this paper, MRR Doppler spectra are reprocessed, exploiting the 2DVD measurements at ground to estimate the effects of vertical winds at 105 m (the most reliable MRR lower height), in order to provide a better estimation of vertical profiles of raindrop size distribution from MRR spectra. Results show that the reprocessing procedure leads to a better agreement between the reflectivity computed at 105 m from the reprocessed MRR spectra and that obtained from the 2DVD data. Finally, vertical profiles of MRR-estimated RSDs and their relevant moments (namely median volume diameter and reflectivity) are presented and discussed in order to investigate the microstructure of rain both in stratiform and convective conditions.

Keywords

Precipitation; Drop size distribution; Vertical profile of reflectivity

1. Introduction

An important property characterizing rainfall is raindrop size distribution (RSD), defined as the concentration of number of raindrops as a function of diameter. Accurate knowledge of RSD is a key factor for understanding precipitation processes and developing and validating precipitation remote sensing retrieval techniques. The characteristics of RSD at ground (such as the shape) result from several different precipitation formation processes (such as coalescence, break-up and drop sorting). Typically, RSD at ground is measured by disdrometers, drop-sampling devices using different measurement principles, such as drop impact (Joss and Waldvogel 1967), video analysis (Schönhuber et al. 2007), laser measurements (Löffler-Mang and Joss 2000), or microwave returns from precipitating particles (Sheppard 1990, and Prodi et al. 2000). However, it is also important to characterize changes of RSD in height, even in layers closer to the ground. Just to mention an application, errors in precipitation estimation from satellite-borne or ground-based weather radar depend also on vertical gradients of RSD in rain (Chandrasekar et al. 2003 and Gorgucci and Baldini, 2015). Investigation of RSD vertical profiles has been conducted with several instruments and methods (e.g., Bringi et al 2009, and Giangrande et al. 2012). Profiler observations, although limited to the rain column above the instruments, have a higher vertical resolution than that achievable by scanning weather radar that varies depending on the distance between radar sample volume and radar antenna. Moreover, they can provide more frequent measurements.

Within the Hydrological Cycle in the Mediterranean Experiment (HyMeX) Special Observing Period 1 (SOP1) framework (Ducroq et al. 2013, and Ferretti et al. 2014 as far SOP1 activities in Central Italy are concerned), a disdrometer and a vertically pointing radar profiler were collocated on a rooftop at Sapienza University of Rome in the historic center of Rome. Specifically, installed were a 2D video disdrometer (2DVD) by Joanneum Research mbH, Graz, Austria (Schönhuber, et al. 2007) and a radar vertical profiler termed Micro Rain Radar (MRR) by Meteorologische

Messtechnik GmbH (Metek). Drop diameter spectra and drop fall velocity spectra measured by 2DVD are considered to be more accurate within all the typical sizes of drops with respect to similar measurements collected by other disdrometers based on different measuring principles (Tokay et al. 2013). The collocated profiling instrument is supposed to provide complementary measurements, referred at different heights of the precipitation column above the instrument. MRR is a relatively cheap frequency-modulated continuous-wave (FM-CW) radar operating at K-band with a low-power solid state transmitter and a 60 cm offset antenna (2° beam width) pointed along a fixed direction. In the configuration adopted in the experiment in Rome, MRR measurements were provided from near ground level (the first gates were not usable) to 1085 meters, with a height resolution of 35 meters, for the purpose of investigating variability of precipitation within a narrow layer close to the surface. MRR estimates power spectra at different heights determined by backscatter of raindrops falling at different velocities. Since fall velocities are related to the diameters of drops, under certain assumptions, MRR spectra can be converted into drop size spectra (Metek 2012). Peters et al. (2005) and Tokay et al. (2009) investigated the performance of MRR using the same configuration adopted in Rome. The first study analyzed the influence of different error sources using theoretical modelling and a dataset composed mainly of light to moderate rain. The second study took advantage of measurements collected by collocated impact disdrometer, raingauge, and an S-band radar profiler during a 16-month experiment. The S-band profiler was taken as reference, being a pulsed system (therefore unaffected by the FM-CW artifacts described later) using an S-band frequency, hence almost unaffected by attenuation and able to provide reflectivity factor measurements in the Rayleigh scattering regime. Reflectivity measured by the S-band profiler agreed quite well with the reflectivity factor (i.e., the sixth moment of estimated raindrop size distribution) obtained from MRR, at a common gate at around 175 m. Moreover, both reflectivities agreed with measurements of an impact disdrometer at ground. However, reflectivity measured by the S-band profiler showed a smaller mean vertical gradient: the mean bias between MRR and profiler reflectivity was within 1 dB for heights below 500 meters. Moreover, the bias

between disdrometer and MRR reflectivity increased both with height and with reflectivity. Such findings suggest that MRR overestimates the vertical variability of reflectivity because of some artifacts related, for example, to spectra aliasing and underestimated attenuation effects.

Successful investigations using MRR in snow and light rain are reported in the literature, although required changes of several aspects of the MRR standard processing chain such as noise level estimation and detection and correction of spectra aliasing and height-Doppler ambiguity (Tridon et al. 2011, Kenifel et al. 2011 and Maahn and Kollias 2012). Conversely, the utility of this instrument in heavy rain or in convection has been questioned (Calheiros and Machado, 2014) and deserves more investigation since heavy rain conditions were frequently observed during the HyMeX SOP 1. For this purpose, HyMeX SOP 1 data were examined to highlight the influence of different factors on vertical profiles estimated by MRR, focusing on heavy rain; also in order to propose some changes in the processing chain to improve the reliability of MRR profiles. The suggested processing takes advantage of techniques already introduced for snow and light rain and of the reference RSD estimated at ground by a disdrometer.

This paper is organized as follows. Section 2 presents an overview of the data available and of the processing of 2DVD and MRR, highlighting and justifying the proposed changes to the standard processing chain of MRR. Results concerning comparison of 2DVD and MRR measurements at the lowest reliable range gates are presented in section 3. Finally, profiles resulting from the HyMeX campaign are illustrated in section 4, while section 5 summarizes important results of the paper.

2. Data and instrumentation

2.1 Overview of the HyMeX SOP 1 measurements in Rome

The study was performed using measurements collected by the MRR and the 2DVD installed on the roof (41.89°N, 12.49°E, 70 m above sea level) of the Department of Electrical Engineering and Telecommunications at Sapienza University of Rome (hereinafter Sapienza site) in the historic center of Rome. A detailed description of instrumentation made available for HyMeX SOP 1 in Central Italy by cooperating institutions for SOP1 is in Ferretti et al. (2014).

Measurements from the two instruments used in this study, namely MRR and 2DVD were available from 4 September to 11 November 2012. Eight days with total rainfall exceeding 5 mm and rain duration exceeding 15 minutes were chosen for this study. Table 1 lists the main characteristics of these rain events revealed by 2 DVD and MRR "averaged data". For each date in the first column (in the format MMDD—2 digits for the month and 2 digits for the day), the number of rainy minutes registered by the two instruments (see sect. 2.2 for a definition of "rainy minute" for 2DVD) is reported in the second column, while the seventh column is the maximum drop diameter detected by the 2DVD during the event. Note that along the manuscript, the subscript "2DVD" means that a quantity has been computed from the 2DVD data, while subscripts like "AVE@105" means that it has been derived from the data provided by the standard Metek processing (namely the "*Averaged data*" described in section 2.3) at the height of 105 m above the ground every minute. Most of the events occurred in September and October were related to the presence of convection, while from the end of October, stratiform precipitation prevailed. Two events in October presented maximum rain rates above 100 mm h^{-1} (Table 1, fifth column), while the longest-lasting event was registered on October 31. In all cases, the melting layer was above the highest gate of the MRR.

2.2 *2DVD processing*

The 2D video disdrometer measures the diameter, fall velocity, and oblateness of individual drops that fall through its virtual measuring area of 10×10 cm^2 (Schönhuber et al. 2007). In order to eliminate spurious drops, namely data potentially affected by instrumental errors or environmental factors (such as wind effect and splashing), the filtering criterion proposed by Tokay et al. (2001) was applied. The criterion implies that drops with velocity outside ±50% of the Atlas et al. (1973) diameter-fall speed relation

$$v_t(D_i) = 9.65 - 10.3\exp(-0.6\,D_i) \qquad (\mathrm{m\,s^{-1}}) \tag{1}$$

were removed. For the selected rain events, the percentage of drops removed by this criterion is reported in the last column of Table 1. For each time interval of duration Δt (s) with more than 10 drops counted, RSD is computed as

$$N(D_i) = \frac{1}{\mathrm{A}\,\Delta t\,\Delta D_i}\sum_{k=1}^{M_i}\frac{1}{v(D_k)} \qquad (mm^{-1}m^{-3}) \tag{2}$$

where ΔD_i (mm) is the width of the *i-th* class of the RSD, *A* is the virtual measuring area in m^2, M_i is the total number of drops detected by the instrument in the *i*-bin, Δt is the time interval (in this paper, Δt can be either 10 seconds or 1 minute), and *v(D)* (m s^{-1}) is the terminal fall velocity of the drops. Although a measurement of fall speed is provided by 2DVD, (1) is used to be consistent with MRR processing. In order to compute the RSD from 2DVD measurements, the detected drops have been stratified in 50 bins with constant width of 0.2 mm and diameters that range from 0 mm to 10 mm.

From the RSD several important hydrological and meteorological observables can be straightforwardly computed, such as the reflectivity factor (*Z*) as

$$Z = \int_{D_{min}}^{D_{max}} N(D)D^6\,dD \qquad (\mathrm{mm^6\,m^{-3}}) \tag{3}$$

where D_{min} and D_{max} are the minimum and maximum drop diameter measured in a given time interval and the median volume diameter D_0 defined by

$$\int_{D_{min}}^{D_0} N(D)D^3\,dD = \frac{1}{2}\int_{D_{min}}^{D_{max}} N(D)D^3\,dD. \quad (4)$$

Furthermore, a characteristic fall velocity can be computed as

$$v_{c,2DVD}(D) = \frac{\int_{D_{min}}^{D_{max}} v_t\,(D)N(D)\,\sigma_b(D)\,dD}{\int_{D_{min}}^{D_{max}} N(D)\,\sigma_b(D)\,dD} \quad (\mathrm{m\ s^{-1}}) \quad (5)$$

where σ_b is the backscattering cross section area computed at a reference frequency, such as that of MRR.

2.3 *MRR standard processing*

The MRR installed in Rome used a 24.243 GHz frequency adopting the FM-CW scheme (Strauch et al. 1976) to estimate Doppler spectra in 64 bins over 32 range gates at a range resolution that depends on the selected width of the linear modulation. Adjusting the frequency modulation between 0.5 and 15 MHz allows one to vary vertical resolution between 300 m and 10 m, respectively. A 35 m resolution was chosen allowing MRR to provide measurements from 0 to 1085 meters. However, the initial and final gates must be excluded because of near field effects and noise, respectively. The peak repetition frequency is fixed to 2 kHz and results in an unambiguous Nyquist velocity range of about 12 m s^{-1}. The MRR standard processing implemented by Metek makes available several types of output: 1) "*Raw data*," provided every 10 seconds, are the lowest level of data available and consist of spectra obtained from 60 frequency sweeps collected in 6-second intervals and additional information to further process them such as the calibration constant and the transfer function. 2) "*Processed data*" are obtained every 10 seconds after processing that includes subtraction of estimated noise level and attenuation correction; outputs include estimated RSD and calculation of some moments,and 3) "*Averaged data*" are similar to "*Processed data*", but are averaged over a longer time interval (typically 60 seconds). The main steps in the procedure to

estimate RSD and its moments are described in Peters et al. (2005), Peters et al. (2010), and Metek (2012). The procedure starts from a matrix of estimated Doppler spectra $S(i,j)$ where i=1, 2, … 64 and j=1, 2, … , 32, are the indices of spectrum lines spaced by 30.25 Hz and range (height) gates, respectively. The first range gate, corresponding to the height of 0 m, is excluded from further processing and therefore is not made available in the "*Processed data*" and "*Averaged data*". Spectra of "*Raw data*" include the contribution of noise that is estimated from consecutive lines in which fluctuation is below a threshold (i.e., the noise level) set from expected fluctuation of noise. For a complete description of the method implemented in the MRR standard process to estimate the noise level see Metek (2012, sect 1.5.2). Estimated noise is subtracted from spectra that are then converted using calibration constant and range weighting into spectral reflectivity density expressed as $\eta_\upsilon(i,j)$ that represent the volume reflectivity in m^{-1} per unit of velocity of each Doppler spectral bin so that the equivalent reflectivity factor at the frequency of MRR at a given range bin can be determined as

$$Z_e = \frac{\lambda^4}{\pi^5 |K_w|^2} \int \eta_v(v)\, dv \quad (\mathrm{mm^6\ m^{-3}}) \tag{6}$$

where K_w is the dielectric factor of water and λ is the radar wavelength. Doppler velocity is converted into drop diameter by inverting the univocal relation between drop diameter and terminal velocity given by (1) that is valid for $0.109 \le D \le 6.109$ mm, corrected for air density vertical gradient using the multiplicative factor $\delta(h) = 1 + 3.68 \times 10^{-5} h + 1.71 \times 10^{-5} h^2$, where h is the height above sea level in meters (Peters et al. 2005). Therefore, the spectral reflectivity density with respect to the drop diameter is given by

$$\eta_D(i,j) = \eta_v(i,j)\ 6.18 \exp(-0.6\, D)\, \delta(h) \quad (\mathrm{mm^{-1}\ m^{-1}}) \tag{7}$$

The obtained spectral lines are relative to diameters given by

$$D(i,j) = \frac{1}{0.6} log \frac{10.3}{9.65 - v_t(i)\delta(h_j)} \quad (\mathrm{mm}) \tag{8}$$

185 that vary with height and are not uniformly spaced. It should be noted that (8) is valid for
186 $0 \leq v_t(i)\delta(h_j) \leq 9.65$ ms^{-1}. For rain, in the absence of updraft or downdraft, such a condition is
187 also verified by larger drops, that, as suggested by, (1) have similar velocities. More precisely, it
188 has been verified that for larger diameters, drop terminal velocity decreases with increasing
189 diameter (e.g., Laws 1941, Beard 1976, Thurai and Bringi, 2005). A downdraft shifts the Doppler
190 spectrum towards higher velocities that could not be inverted by (8). Therefore (8) is applied only
191 to diameters *D* within the range limits of 0.246 mm and 5.8 mm corresponding to velocities
192 between 0.76 m s^{-1} and 9.36 m s^{-1}. This fact implies that MRR estimated RSDs are truncated.
193
194 Then, assuming that drops are oblate spheroids of equivalent volumetric spherical diameter *D*, the
195 single particle backscattering cross-section is calculated under Mie theory and used to normalize
196 power spectra to become profiles of RSDs from which the profiles of the various moments are
197 obtained. Among the moments calculated, the reflectivity factor is the sixth moment of the RSD as
198 in (3), which is not the same as the equivalent reflectivity factor for the MRR frequency computed
199 by (6).
200 A critical processing step to obtain meaningful RSD profiles is the correction of attenuation that, at
201 the MRR frequency, can be important. The attenuation correction method used, which is based on
202 the Hitschfeld and Bordan (1954) algorithm, is applied until path integrated attenuation (PIA) does
203 not exceed 10 dB because for higher attenuation, possible miscalibration can produce unreliable
204 corrections (Peters et al., 2010). In fact, attenuation is estimated recursively using RSD estimates to
205 obtain, using extinction cross-sections for each diameter bin, specific attenuation at each gate.
206 Therefore incorrect RSD estimation leads to incorrect specific attenuation estimation that can
207 propagate along height in the PIA. This aspect suggests that in the case of intense precipitation,
208 MRR estimates become less reliable at increasing height.

2.4 MRR new processing

We propose an improvement over the MRR standard processing focused on intense rainfall. The MRR raw spectra ("*Raw data*") are used as a starting point. The MRR new processing proposed in this study has five main steps. For each time interval we:

1) estimate the noise level of each raw spectrum in the different range gate;

2) unfold the spectrum affected by aliasing;

3) compare the characteristic fall velocity of 2DVD (5) with the one obtained from the MRR spectra at 105 m above the ground level (9);

4) estimate the RSDs at the different elevations;

5) apply an attenuation correction algorithm.

In the following each step of the proposed processing is described in detail.

For the first step, we employed the noise estimation technique of Maahn and Kollias (2012), which aims at improving sensitivity of MRR in snow or light rain measurements. With respect to the MRR standard procedure, removal of isolated noise peaks is obtained, as shown in Figure 1, that compares reflectivity spectra of standard "*Processed data*" (a) with the corresponding spectra obtained having applied the Maahn and Kollias (2012) procedure (b). Note that a spectrum line around 1000-m height is missing in the "*Processed data*". This comparison allows us to introduce further processing steps. In fact, Figure 1 also highlights the presence of spectrum aliasing. Aliasing occurs when velocity exceeds the Nyquist velocity boundaries of 0 and +12 m s^{-1}. Actually, if the Doppler spectrum is generated by fall velocities in still air, it should be limited between 0 and 9.65 m s^{-1}. Figure 1 shows a truncation on the left part of the spectrum and non-null spectrum close to the right side due to the likely presence of downdraft. This is a clear indication of the presence of aliasing.

The impact of aliasing has been investigated by Kneifel et al. (2011) and Maahn and Kollias (2012) for snow, for which the likely presence of negative velocities (e.g., -1 m s^{-1}) resulting from updrafts

is wrongly interpreted as particles falling at high speed (i.e., 11 m s^{-1}). In heavy precipitation a portion of the Doppler spectra can exceed the Nyquist velocity boundaries in the presence of downdrafts. Moreover, when Nyquist velocity boundaries are exceeded, the particle whose velocities exceed the upper boundary contributes to the spectrum in the closer range gate (Ince, 2009). Starting from this statement, the approach followed in this study to reveal the presence of aliasing and to unfold the spectra entails consideration of three adjacent spectra increasing the velocity range from -12 ms^{-1} to 24 ms^{-1}. This approach is similar to the one proposed by Maahn and Kollias (2012) and is applied to each time interval independently. Assuming that we are applying the dealiasing procedure to the spectrum of the *j*-th range gate, the triplicated spectrum, will be composed of the spectrum at the *j*-th height gate, the one measured at the lower (*j*−1)-th and the one at the upper (*j*+1)-th range gate (see Figure 2). Therefore this spectrum contains up to three peaks with different Doppler velocities. First we identified the peak of the spectrum at the *j*-th range gate (namely the one with fall velocities between 0 ms^{-1} and 12 ms^{-1}). Then starting from this peak we search the upper and lower limits of the *j*-th spectrum. The lower (or upper) limit of the *j*-th spectrum is identified as the first bin between the peak of the *j*-th spectrum and the peak of the (*j*−1)-th (or (*j*+1)-th) spectrum with a value of spectral reflectivity lower than the noise level (estimated with the procedure mentioned above), or, if it does not exist, with the bin corresponding to the minimum values of the spectral reflectivity. Once the lower and upper limits of the spectrum have been defined all the bins outside the latter limits are masked.

The presence of updraft or downdraft does not necessarily determine aliasing of spectra, but simply a shift that, jointly with the truncation, determines a wrong shape of the retrieved RSD that can have a different impact on the different RSD moments. In fact, one of the main assumptions used in the MRR standard processing to retrieve the RSD is the absence of vertical wind; under these condition the mean Doppler velocity is related only to the hydrometeor fall speed. In practice,

during convection or in the presence of up/down draft the mean Doppler velocity is composed of not only the hydrometeor fall speed but also the air velocity; therefore, the retrieved RSD can be biased. Peters et al. (2005) studied the effects of the vertical wind on the retrieved RSD and rainfall parameters and found that the relation between rain and reflectivity (both the equivalent reflectivity from (6) or the one estimated from (3)) is not changed significantly, even for rain rates close to 100 mm h^{-1}, but only for very low values of the vertical winds (i.e. in the range ±0.76 m s^{-1}). For higher values, like those usually registered during convection, effects on the retrieved RSDs are expected to be more relevant.

The approach proposed in this study for retrieving the RSD in the presence of vertical wind consists of considering the 2DVD as a reference and shifting the MRR spectral reflectivity until it has the same characteristic fall velocity computed from the 2DVD data. For each time interval (10 seconds), the 2DVD characteristic fall velocity is computed with (5), while the MRR characteristic fall velocity, that is the first moment of the Doppler spectrum, is computed as

$$v_{c,MRR} = \frac{\int \eta_v(v)\, v\, dv}{\int \eta_v(v)\, dv} \quad (\mathrm{m\ s^{-1}}) \tag{9}$$

in the spectral reflectivity domain. The spectrum used in (9) is the one obtained after the dealiasing. It should be noted that $v_{c,MRR}$ is independent on attenuation and calibration, and should be equal to $v_{c,2DVD}$ defined by (5). For each time interval, we directly compare the characteristic fall velocity of 2DVD and the one of MRR at 105 m (third range gate). The latter has been computed with (9) using 10-sec spectrum obtained at 105 m after the application of noise level and aliasing correction explained above. In this comparison, we assume that the vertical change in RSD within the lowest 100 m is negligible (between the third range gate of the MRR and the 2DVD), and that the vertical motions are near zero at the height of the 2DVD measurements (at ground). Therefore, the difference between the 2DVD measured characteristic fall velocity and the MRR characteristic fall velocity at 105 m can be ascribed to the presence of up/down draft. Assuming that the up/down draft does not vary significantly within the lowest 1 km AGL (the maximum MRR measurement

284 height; e.g. May and Rajopadhyaya 1999, Giangrande et al. 2013), we can use this difference to
285 remove the up/down draft from the MRR velocity measurements at all the range gates. For a given
286 time interval, the correction described above is applied only to MRR spectra for which the
287 difference between the two characteristic velocities (namely those obtained from the 2DVD and the
288 one obtained from the MRR spectrum at 105 m) exceed ± 0.2 m s^{-1} that corresponds to the
289 resolution of MRR Doppler spectra. Once the MRR raw spectra have been corrected for noise level,
290 for aliasing, and for the presence of vertical wind, the spectral reflectivity density with respect to
291 drop diameter can be obtained by (7) and, finally, the RSD can be computed, normalizing the
292 spectra by the single particle backscattering cross-section calculated under Mie theory. Finally, the
293 technique for attenuation correction discussed in details in Peters et al. (2010) was applied. Spectra
294 with path integrated attenuation greater than 10 dB, were discarded. Note that hereinafter the term
295 NEW@105 means the RSDs and the corresponding parameters (such as the reflectivity factor)
296 obtained at 105 m above the ground level after the application of the MRR new processing
297 procedure proposed in this section.
298 The steps of the MRR new processing and of the MRR standard processing are summarized in
299 Figure 3 where differences and similarities between the two procedures are underlined. As
300 example, in Figure 2 shown are the effects of the new steps introduced in the processing of the
301 MRR raw spectra, namely the dealiasing (in Figure 3 step 2 of the MRR new processing), and the
302 correction for the presence of vertical wind (in Figure 3 step 3 of the MRR new processing). The
303 solid black line reported in Figure 2 represents the corrected spectrum as resulted from the MRR
304 new processing proposed in this study and it is the spectrum used to compute the RSD.

305 **3. Validation of MRR estimated RSD with 2DVD**

306 Following the procedure described in section 2.4, for each time interval, the RSD can be obtained
307 for all height gates (from 35 m to 1085 m), from the MRR raw spectra and the corresponding
308 integral rainfall parameters can be computed. After the application of the proposed MRR new

processing procedure the obtained spectra can be considered dealiased and unaffected by the presence of vertical wind. To validate the procedure of section 2.4, the reflectivity estimated from the MRR data at 105 m (third range gate) has been compared with the one obtained at the same time interval from the 2DVD data. To perform a meaningful comparison, it should be taken into account that the 2DVD have a much smaller sampling volume than the MRR (5 orders of magnitude of difference) and that there is a time shift due to the raindrop fall velocity between measurements at 105-m height and at ground. To reduce possible time mismatching, measurements are compared by considering Δt = 1 minute and, therefore, MRR "*Averaged data*" are used. It should be noted that reflectivity factors compared in this section are D^6-based and computed using (3) considering the RSDs measured by 2DVD or estimated by MRR. The statistical estimators used to quantify the goodness of the comparison are the normalized standard error (*NSE*)

$$NSE = \frac{\sqrt{\overline{(x-y)^2}}}{\bar{x}} \tag{10}$$

Normalized bias (*NB*)

$$NB = \frac{\sum y}{\sum x} - 1 \tag{11}$$

and correlation coefficient (*cc*)

$$cc = \frac{\overline{(x \cdot y)} - (\bar{x} \cdot \bar{y})}{std(x) \cdot std(y)} \tag{12}$$

where x and y are the dependent and independent variables, respectively.

Table 2 shows the values of those estimators where *x* is the reflectivity factor computed from the 2DVD data and *y* is *i)* the reflectivity at 105 m provided by the MRR standard processing in the "*Average data*" file, referred to as AVE@105, (fourth, fifth, and sixth columns), or *ii)* the reflectivity factor at 105 m obtained from the RSD estimated applying the MRR new processing described in section 2.4 to the MRR raw spectra, referred to as NEW@105 (seventh, eighth, and

ninth columns). Note that the reflectivities in (10), (11), and (12) are in linear scale. A negative value of *NB* means underestimation of MRR with respect to the reference measurements of the 2DVD, while higher *NSE* values mean a higher discrepancy between the MRR and 2DVD measurements. The values of *NSE, NB*, and correlation coefficient obtained after the application of the proposed processing are in general better than the ones obtained comparing the 2DVD with the "*Averaged data*" (AVE@105). This trend is verified for all the cases considered from the HyMeX SOP 1 campaign shown in Table 1. Note that only in one case (1031) the improvement of the *NSE* is not obtained, although a considerable decrease of *NB* is reached. Normalized bias that ranged between -6.5 dB and -2.1 dB for the AVE@105, with the processing procedure exposed in section 2.4 varies between -1.7 dB and 0.9 dB, thus reducing the underestimation of reflectivity. Notably, a reduction of *NB* of more than 5 dB is achieved for the case of October 15, a convective event. Having assumed the 2DVD as a reference, the latter results indicate that the proposed processing improves the retrieval of the RSD and reflectivity from the MRR raw spectra. The scatterplot of Figure 4 compares the reflectivity of 2DVD with the reflectivity derived by the MRR standard processing for 1 minute resolution at the third range gate (AVE@105) and with the reflectivity of MRR at 105 m using the proposed MRR new processing (NEW@105). The proposed processing allows a better agreement with the 2DVD, as shown by reflectivity factor estimates more clustered along the identity line for all the range of values. Note that in order to analyze the latter results in relation with the type of rainy event in Table 2 (second and third columns) the percentages of 1-min RSDs classified as convective and stratiform rain, respectively, are provided. To classify the minutes of the rain event (stratiform, convective or transition) we applied the Stratiform/Convective (C/S) algorithm proposed by Bringi et al. (2009) to the 2DVD data. The latter algorithm employs two RSD parameters: N_w, namely the intercept parameter of a normalized gamma RSD, and D_o, namely the median value of the volumetric size spectra.

Spectra measured by 2DVD and MRR at 105 m are compared in Figure 5. The 2DVD spectra were obtained by stratifying the selected drops (see section 2.2) into 50 bins with constant width (ΔD = 0.2 mm) from 0 mm to 10 mm. For each rain event, all the RSDs measured by the 2DVD were averaged (solid black lines) and compared with the event RSD computed averaging the RSDs at 105 m provided by the MRR standard processing, namely AVE@105, (dashed grey lines in Figure 5) and with the event-averaged RSD estimated using the MRR new processing procedure, namely NEW@105, (solid grey lines in Figure 5). It should be noted that some RSDs reported in the "*Averaged data*" files have unrealistic values. In order to obtain a feasible averaged RSD, the spectra with values higher than 10^{10} mm^{-1} m^{-3} were eliminated and not consider for further analysis. The event-averaged RSDs shown in Figure 5 can be analyzed over three different diameter ranges: small drops (D < 1 mm), midsize drops (1 mm < D < 4 mm), and large drops (D > 4 mm). The RSDs obtained through the new processing are in better agreement with the 2DVD, in particular for the midsize raindrops. Relative to the 2DVD, the dealiasing technique employed on MRR measurements still produces an overestimation of the number of small drops and underestimation of the number of large drops. It must be remembered that the MRR can detect drops in the range 0.246 mm ≤ D ≤ 5.8 mm, while the 2DVD theoretically can detect drops up to 10 mm in diameter. However, the very large drops (D > 5 mm) occur quite rarely. Furthermore, due to instrument resolution, the 2DVD may underestimate the small drops with D < 0.5 mm (Tokay et al. 2013) and therefore the discrepancy for such diameters can be ascribed also to the 2DVD and not only to the MRR.

4. Vertical profiles of RSD parameters

In this section vertical profiles of rainfall parameters and RSD obtained applying the processing procedure presented in section 2.4 from the MRR raw spectra are shown for significant events among the eight listed in Table 1. In case of intense precipitation, 24-GHz attenuation can play a role in degrading the performance of MRR retrieval as suggested by Tokay et al. (2009). The

attenuation correction technique described in Peters et al. (2010) can fail because of effects like wrong calibration of MRR. Therefore some conclusions of this section are drawn in a qualitative way. All the profiles are below the bottom of the melting layer for all the considered events. Most of the studies on MRR vertical profiles available in the literature focus on more extended elevation range, in particular those aiming at identifying phases of precipitation through the detection of signatures of melting layer. As far as profile below the melting layer is concerned, it is typically modelled as nearly constant also in convective rain (e.g. Kirstetter et al. 2013, and Le and Chandrasekar 2014). Figure 6a,c show two examples of time series of reflectivity vertical profiles obtained through the MRR new processing. Figure 6a shows the vertical profile of the reflectivity factor during a convective rain event occurred on 15 October 2012. A quite high vertical variability of the radar reflectivity derived by the MRR data can be noted between 1800 and 1816 UTC along with high values of Z (up to 55 dBz) near the ground level. After 1816 UTC, the reflectivity obtained from MRR is lower and more constant with height, suggesting a stratiform phase, although it is not possible to identify the signature of the bright band because it is located higher than the maximum height of MRR. However, a deeper discussion of this event will be presented later. Finally, Figure 6c shows the vertical profile of reflectivity during more than four of the eight hours of continuous stratiform rain measured by MRR during a long-lasting rain event (916 minutes) that occurred on 31 October 2012. The values of Z appears to be almost constant with the height and range between 20 dBz and 40 dBz. Figure 6b,d show the time series of the reflectivity factor *i)* obtained from the 2DVD data, *ii)* estimated at the reliable gate closest to the ground level, 105 m, namely NEW@105, and *iii)* provided by Metek in the "*Averaged data*" files, namely AVE@105. The reflectivity factor at 105 m obtained through the MRR new processing is in better agreement with the one computed from the RSDs collected by 2DVD respect to the reflectivity factor provided by the MRR standard processing. The improvement of the MRR new processing in terms of Z is more evident for the convective event (Figure 6b) than for the stratiform one (Figure 6d).

The most interesting convective event (and, consequently most challenging for our analysis) among those observed during HyMeX SOP 1 was that occurred in Rome on 15 October 2012, when a frontal system moved rapidly toward Italy, causing moist air advection over the Tyrrhenian Sea and a consequent convection. Along with the vertical profile of the reflectivity, the vertical profiles of rain microstructures, such as drop size distribution and D_0 (mm) computed using (4), during the convective and the stratiform phase of the event are reported and discussed. Focus on Z and D_0 is because they are frequently used in the literature to classify the two precipitation regimes from disdrometers and dual-polarization radar observations (e.g. Maki et al., 2001, Rosenfeld and Ulbrich, 2003, Bringi et al., 2009). On 15 October 2012, 189 rainy minutes were recorded by both devices, and applying the Bringi et al. (2009) C/S algorithm to the 2DVD data, we obtained 26 minutes of convective rain and 160 minutes of stratiform rain, while three minutes were classified in the transition region between the two regimes (see Table 2). Figure 7 shows the vertical profiles of Z for the stratiform (a) and convective (b) phases of the rain event from 105 m (third range gates) to 1085 m. While in Figure 8 are reported the vertical profiles of D_0 in the two different rain regimes, namely stratiform (a) and convective (b). Note that only the complete profile are considered in the box plots of Figure 7 and Figure 8 . From the radiosondes data of Pratica di Mare (30 km south of instrumented site) we know that the height of the 0° isothermal was at 2810 m ASL at 1200 UTC and therefore, the MRR is not able to reveal the bright band signature. During convection, large drops are more frequent, and therefore the values of Z and D_0 are expected to be higher than the ones measured during stratiform rain: the median value of Z at 105 m is 25.5 dBz for stratiform rain and 46.4 dBz for convective rain, while the median values of the mean drop diameter are 0.98 mm and 2.07 mm, respectively. Figure 7a shows that the mean reflectivity profile during the stratiform phase of the event is almost constant with height. Approximating vertical profiles with lines, the median slope is -1.4 dB km^{-1} (25^{th} and 75^{th} percentiles are -6.8 and 3.7 dB km^{-1}), almost independently on the reflectivity at 105 meters. During the convective phase of the event, the reflectivity monotonically decreases (from 46.4 dBz to 30.9 dBz) with height, presenting

higher vertical gradient that appears to depend on the reflectivity (Figure 7b). For profiles with reflectivity at 105-m height between 35 and 45 dBZ, median slope is -9.0 dB km^{-1}, while for the interval between 45 and 55 dBZ, median slope is -23.8 dB km^{-1}. Without a reference profile it is not easy to determine the specific influence of gradients in vertical wind or uncompensated attenuation. Figure 8a shows that during the stratiform rain the vertical profiles of D_0 are almost constant within 1 km of the AGL layer (i.e., the median values are 0.98 mm at 105 m and 0.84 mm at 1050 m), while during convection the mean drop diameter monotonically decreases with height up to 500 m AGL and then it is almost constant (Figure 8b). The median D_0 of convective minutes is 2.07 mm at 105 m AGL, 1.26 mm at 525 m AGL, and 1.25 mm at 1050 m AGL. The increase of D_0 from about 500 m AGL to the ground level means that the number of large drops increase with respect to the small drops: in other words, drops become larger in diameter. The latter behavior can be due to drop sorting and to the predominance of the coalescence process in this height range (Porcù et al., 2012). However, there is a huge difference in the variability of D_0 with height. In fact, supposing a linear D_0 vertical gradient, we get an average value of -0.7 mm km^{-1} and -0.2 mm km^{-1} for convective and stratiform rain, respectively, associated to a residual error of 3.0 mm km^{-1} and 0.6 mm km^{-1}, respectively. In practice the high values of the residual error for the convective case, means that variability along the vertical can span the entire variability of D_0, at least for 10-s spectra. However, attenuation correction can somehow contribute to this apparent effect.

In order to compare average behavior of RSD for the different phases of the storm, Figure 9 shows the vertical profile of RSDs averaged over the 160 stratiform minutes (a) and over the 26 convective minutes (b) of the rain event of 15 October 2012. The vertical RSD profiles presented different shapes during the convective and the stratiform phases. During the stratiform phase the RSDs did not change significantly with the height and there were fewer small and large drops than those recorded during the convective phase. Conversely, during the convective phase (Figure 9b), the RSD changes with height, in particular below 400-500 m AGL. Below this height, the number of midsize and large drops increased toward the ground level, perhaps largely due to coalescence

and drop sorting. Note also that D_0 increased in this height range during convective rain (Figure 8b). Although the vertical 1-min RSD profiles appear to be noisier, the behavior identified for the stratiform and convective rain is still evident.

5. Summary and conclusions

Several experiments aiming at investigating raindrop size distribution at ground level and their variation with height deployed instruments like disdrometers and radar profilers close each other. Within experiments carried out in Italy in autumn 2012 in the framework of the HyMeX SOP 1 a 2DVD video disdrometer and a micro rain radar were installed in the historic center of Rome. The MRR was configured to provide RSD estimates with a height resolution of 35 m within 1085 m above the ground. While 2DVD is considered to be an accurate instrument for measuring RSD at ground, the quality of MRR measurements in heavy rain or convection deserve more investigation. The dataset collect during the experiment in Italy, from which 8 rainy days were selected, includes a couple of days with maximum rain rates exceeding 100 mm h^{-1}. A number of issues, such as the K-band frequency that suffers from attenuation even in moderate rain, the validity of assumption of still air adopted by the MRR standard processing, are sources of error that affect the vertical profiles of MRR retrieved RSD. Since RSD retrieval is based on converting Doppler spectra into drop size spectra via a well-known experimental relation valid in still air, vertical winds produce a shift in MRR measured Doppler spectra that translate into an error in the retrieved RSD that will result both shifted and with a different shape. MRR raw spectra have been analyzed in order to highlight impact of possible sources of error in RSD retrieval and to design an improved processing. Several improvements have been made to the MRR standard processing chain, owing to existing literature, such as the estimation of noise level and the correction of spectra aliasing and range-Doppler ambiguities. A novel step introduced in this paper focuses on the effect of vertical wind and consists in constraining the characteristic fall velocity of MRR at a reliable low height

481 gate (namely that at 105 meters) to that obtained from 2DVD measurements. Results show an
482 important improvement, in terms of normalized bias, normalized standard error and correlation
483 coefficient between the reflectivity computed from the 2DVD data and the one computed from
484 MRR spectra at 105 m AGL. In particular, comparing the *NSE* obtained from the MRR standard
485 procedure (namely AVE@105) and the proposed MRR new processing (namely NEW@105), a
486 decrease between 5% and 50%, depending on the event, is obtained. Even a higher reduction is
487 obtained for the *NB*, while the correlation coefficients increase. Such results show on one hand that
488 the suggested procedure improves the robustness of RSD estimate obtained at 105 m by the MRR,
489 and on the other, that vertical winds are a major source of error in rain. The MRR new processing
490 allows to correct all the spectra of the precipitation column within the maximum range of MRR
491 assuming that vertical wind is constant within 1 km AGL, although such assumption can be
492 questionable in convection. The proposed processing procedure would aim to consider as more
493 reliable the spectra estimated by MRR at different heights in all rain condition, allowing to
494 investigate the microstructure of rain both in stratiform and convective conditions. For one of the
495 convective events investigated in this study, statistics of vertical profiles of reflectivity, drop size
496 distribution and volume median diameter were shown after partitioning minutes of precipitation in
497 stratiform and convective. However, a validation of profile retrievals would require some reference
498 profiling instruments that were not available during HyMeX SOP1. Therefore, being not possible to
499 compare the vertical profile of MRR derived RSDs or relative moments to those obtained by a
500 different instrument, only qualitative conclusions can be drafted. Different shapes of RSD profiles
501 were found depending on the type of precipitation (stratiform/convective). Such differences were
502 highlighted also by the trends with height of reflectivity or D_0 that show different behavior
503 depending on the stratiform/convective classification. Supposing that vertical profiles can be
504 linearly approximated, the slope of reflectivity profile shows a certain dependence on Z at the
505 reference height (105 meter) in convection, namely increasing (in absolute value) as reference
506 reflectivity increases. It is not easy to determine the contribution to this behavior to precipitation

physics or to artifacts of the retrieval technique, particularly, effects of vertical wind and attenuation correction. More sensitive to stratiform/convective classification appears to be D_0 that exhibits in convection an extremely high variability with height that suggest a scarce accuracy of MRR technique to retrieve such parameter in convection at maximum time resolution (10 sec). As mentioned above, further investigation of the impact of wind velocities varying with height would require reference profiling instruments.

Acknowledgments

This research has been carried out as a contribution to the SOP 1 of the HyMeX program. The setup of instruments in Rome was possible thanks to cooperation among DIET-Sapienza University of Rome (Prof. F. S. Marzano), NASA-GSFC, and the HyMeX coordination. The authors acknowledge the anonymous Reviewers for their detailed and helpful comments to the manuscript. The authors also acknowledge the ground validation program of the NASA Global Precipitation Measurement (GPM) mission under Matthew Schwaller and Walter A. Petersen, GPM ground validation and science manager, respectively, for providing instruments and expertise, and Arthur Hou, former GPM project scientist (deceased), who promoted the participation of NASA to HyMeX SOP 1.

References

Atlas, D., Srivastava, R. C., Sekhon, R. S., 1973. Doppler radar characteristics of precipitation at vertical incidence. Rev. Geophys. Space Ge., 11, 1-35.

Beard, K. V., 1976. Terminal velocity and shape of cloud and precipitation drops aloft. J. Atmos. Sci. 33, 851-864. Doi: 10.1175/1520-0469(1976)033%3C0851:TVASOC%3E2.0.CO;2

Beard, K. V., Chuang, C., 1987. A new model for the equilibrium shape of raindrops. J. Atmos. Sci. 44, 1509-1524. Doi: 10.1175/1520-0469(1987)044<1509:ANMFTE>2.0.CO;2

Bringi V. N., Chandrasekar V, Hubbert J., Gorgucci E., Randeu W. L., Schoenhuber M., 2003. Raindrop size distribution in different climatic regimes from disdrometer and dual-polarized radar analysis. J. Atmos Sci. 60, 354-365. Doi: 10.1175/1520-0469(2003)060<0354:RSDIDC>2.0.CO;2.

Bringi V. N., Williams C. R., Thurai M., May P. T., 2009. Using dual-polarized radar and dual-frequency profiler for DSD characterization: a case study from Darwin, Australia. J. Atmos. Oceanic Technol. 26, 2107–2122. Doi: 10.1175/2009JTECHA1258.1

Calheiros A. J. P., Machado L. A. T., 2014. Cloud and rain liquid water statistics in the CHUVA campaign. Atmos Res. 144, 126-140. Doi: 10.1016/j.atmosres.2014.03.006.

Chandrasekar, V., Meneghini R., R. Zawadzki, I., 2003. Global and local precipitation measurements by radar. Meteorological Monographs. 30, 215–215. Doi: 10.1175/0065-9401(2003)030<0215:GALPMB>2.0.CO;2

Ducrocq V., et al. 2013. HyMeX-SOP 1, the field campaign dedicated to heavy precipitation and flash flooding in the northwestern Mediterranean. Bull. Amer. Meteor. Soc. 95, 1083–1100. Doi: 10.1175/BAMS-D-12-00244.1

Ferretti R. et al., 2014. Overview of the first HyMeX Special Observation Period over Italy: observations and model results. Hydrol. Earth Syst. Sci. 18, 1953-1977. Doi:10.5194/hess-18-1953-2014.

548 Giangrande S. E., Luke E. P., Kollias P., 2012. Characterization of vertical velocity and drop size
549 distribution parameters in widespread precipitation at ARM facilities. J. Appl. Meteor. Climatol. 51,
550 380–391. Doi: 10.1175/JAMC-D-10-05000.1.

551 Giangrande, S. E., Collis S., Straka J., Protat A., Williams C., and Krueger S., 2013: A summary of
552 convective-core vertical velocity properties using ARM UHF wind profilers in Oklahoma. J. Appl.
553 Meteor. Climatol., 52, 2278–2295, doi:10.1175/JAMC-D-12-0185.1.

554 Gorgucci E., Baldini L., 2015. Influence of beam broadening on the accuracy of radar polarimetric
555 rainfall estimation. J. Hydrometeor. (in press) doi: http://dx.doi.org/10.1175/JHM-D-14-0084.1.

556 Hitschfeld, W., Bordan J., 1954. Errors inherent in the radar measurement of rainfall at attenuating
557 wavelengths. J. Meteor. 11, 58–67. Doi: 10.1175/1520-0469(1954)011<0058:EIITRM>2.0.CO;2

558 Ince, T., 2009. On Performance of S-band FMCW Radar for Atmospheric Measurements,
559 Advances in Geoscience and Remote Sensing, Gary Jedlovec (Ed.), InTech, Doi: 10.5772/8320.

560 Joss, J., Waldvogel, A.. 1967. Ein spectrograph für Niederschlasgstropfen mit automatischer
561 Auswertung (A spectrograph for the automatic analysis of raindrops). Pure Appl. Geophys., 69,
562 240–246.

563 Kirstetter, P. E., Andrieu, H. Delrieu, G. Boudevillain, B.. 2013: A physically based identification
564 of vertical profiles of reflectivity from volume scan radar data. J. Appl. Meteor. Climatol., 52,
565 1645–1663, doi:10.1175/JAMC-D-12-0228.1

566 Kneifel, S., Maahn, M., Peters, G., Simmer, C., 2011. Observation of snowfall with a low-power
567 FM-CW K-band radar (Micro Rain Radar), Meteorol. Atmos. Phys. 113, 75–87. Doi:
568 10.1007/s00703-011-0142-z.

569 Laws, J. O., 1941. Measurements of the fall-velocity of water-drops and raindrops. Transactions,
570 American Geophysical Union, 22, 709-721. Doi: 10.1029/TR022i003p00709.

Le, M., Chandrasekar, V., 2014. An algorithm for Drop-Size Distribution retrieval from GPM Dual-Frequency Precipitation Radar. IEEE T. Geoscience and Remote Sensing, 52, 7170-7185. http://dx.doi.org/10.1109/TGRS.2014.2308475.

Löffler-Mang, M., Joss, J., 2000. An optical disdrometer for measuring size and velocity of hydrometeors. J. Atmos. Oceanic Technol., 17, 130–139.

Maahn, M., Kollias, P., 2012. Improved Micro Rain Radar snow measurements using Doppler spectra post-processing. Atmos. Meas. Tech., 5, 2661-2673.

Maki, M., Keenan, T. D., Sasaki, Y., Nakamura, K., 2001. Characteristics of the raindrop size distribution in tropical continental squall lines observed in Darwin, Australia. J. Appl. Meteor. 40, 1393–1412. Doi: 10.1175/1520-0450(2001)040<1393:COTRSD>2.0.CO;2

May, P. T., and Rajopadhyaya D. K., 1999: Vertical velocity characteristics of deep convection over Darwin, Australia. Mon. Wea. Rev., 127, 1056–1071.

METEK, 2012., MRR Physical Basics, (Update of 13 March 2012) Elmshorn, 20 pp., Metek mbH.

Peters, G., Fischer, B., Münster, H., Clemens, M., Wagner, A., 2005. Profiles of raindrop size distributions as retrieved by Microrain Radars, J. Appl. Meteorol. 44, 1930–1949. doi: 10.1175/JAM2316.1

Peters, G., Fischer, B., Münster, H., Clemens, M., 2010. Rain attenuation of radar echoes considering finite ‐ range resolution and using drop size distributions, J. Atmos. Ocean. Technol. 44, 829–842. doi: 10.1175/2009JTECHA1342.1

Porcù, F., D'Adderio, L. P., Prodi, F., Caracciolo, C., 2012. Effects of altitude on maximum raindrop size and fall velocity as limited by collisional breakup. J. Atmos Sci. 70, 1129-1134. doi:10.1175/JAS-D-12-0100.1.

Prodi, F., Tagliavini, A., Pasqualucci, F., 2000. Pludix: An X-band sensor for measuring hydrometeors size distributions and fall rate. Proc. 13th Int. Conf. on Clouds and Precipitation, Reno, Nevada, ICCP and IAMAS, 338–339.

Rosenfeld, D., Ulbrich, C. W., 2003. Cloud microphysical properties, processes, and rainfall estimation opportunities. Meteor. Monogr. 52, 237-258. Doi: 10.1175/0065-9401(2003)030<0237:CMPPAR>2.0.CO;2

Schönhuber, M., G. Lammer, and W. L. Randeu, 2007: One decade of imaging precipitation measurement by 2D-video-disdrometer. Adv. Geosci., 10 , 85-90

Sheppard, B.E., 1990: Measurement of raindrop size distributions using a small Doppler radar, J. Atmos. Oceanic Technol., 7, 255-268.

Strauch, R. G., Campbell, W. C., Chadwick, R. B., Moran, K. P., 1976. Microwave FM-CW Doppler radar for boundary layer probing. Geophys. Res. Lett. 3, 193-196.

Thurai, M., Bringi, V. N., 2005. Drop axis ratios from a 2D video disdrometer. J. Atmos. Oceanic. Technol., 22, 966-978.

Tokay, A., Kruger, A., Krajewski, W. F., 2001. Comparison of drop-size distribution measurements by impact and optical disdrometers. J. Appl. Meteorol., 40, 2083-2097.

Tokay, A., Hartmann, P., Battaglia, A., Gage, K. S., Clark, W. L., Williams, C. R., 2009. A field study of reflectivity and Z–R relations using vertically pointing radars and disdrometers. *J. Atmos. Oceanic* Technol. 26, 1120–1134, doi:10.1175/2008JTECHA1163.1.

Tokay A., Petersen W. A., Gatlin P., Wingo M., 2013. Comparison of raindrop size distribution measurements by collocated disdrometers. J. Atmos. Oceanic Technol. 30, 1672–1690, doi:10.1175/JTECH-D-12-00163.1.

Tridon F., Baelen J. V., Pointin Y., 2011. Aliasing in Micro Rain Radar data due to strong vertical winds. Geophys. Res. Lett., 38, 4773 – 4793. doi:201110.1029/2010GL046018.

Table Captions

Table 1: Summary of 2DVD and MRR recordings during HyMeX SOP 1 in Rome.

Table 2: Values of normalized standard error (NSE; dimensionless), normalized bias (NB; dimensionless and in dB in brackets), and correlation coefficient (cc; dimensionless) between i) the reflectivity factor computed from the data recorded by the 2DVD and that provided by the MRR standard processing ("Averaged data") at 105 m (AVE@105), and ii) the reflectivity factor computed from the data recorded by the 2DVD and the reflectivity computed from the RSD at 105 m obtained after the application of the new processing of the MRR raw spectra (NEW@105) (see section 2.4).

628

629 **Figure Captions**

630 Figure 1: Reflectivity spectra provided by Metek in “Processed data” file on 15 October 2012 at
631 18:01:27 UTC (a) and reflectivity spectra obtained applying the noise removal procedure proposed
632 by Maahn and Kollias (2012) to the raw spectra (b).

633 Figure 2: Example of the effects of the dealiasing and the correction for the presence of the vertical
634 wind. The spectrum at 105 m at 17:58:57 UTC of 12 October 2012 is plotted with solid grey lines
635 and circles and represents the j-th to be corrected. For the dealiasing procedure the (j-1)-th (namely
636 at 70 m) and (j+1)-th (namely at 140 m) are considered (solid grey lines) and as result of this step,
637 the dealiased spectrum is obtained and plotted with dashed black line. Finally, the solid black line is
638 the dealiased spectra after the shift due to the presence of the vertical wind. The solid horizontal
639 lines represent the Nyquist velocity boundaries (0 and +12 ms-1), namely the limits of the jth
640 spectrum, while the dashed horizontal lines are the velocity range for the RSD retrieval, namely v =
641 0.76 ms-1 and v = 9.36 ms-1.

642 Figure 3: Flowchart of the processing steps involved in the MRR standard processing (on the left)
643 and the MRR new processing (on the right).

644 Figure 4: Scatterplot comparing reflectivity factor from 2DVD spectra with i) reflectivity factor of
645 MRR standard product at 105 m, namely AVE@105, (grey dots), and ii) reflectivity factor of MRR
646 using the processing approach proposed in this study, namely NEW@105, (black dots).

647 Figure 5: Averaged RSD obtained from 2DVD data (black solid lines), MRR “Averaged data” at
648 105 m, namely AVE@105, (dashed grey lines), and MRR raw spectra reprocessed following the
649 new procedure proposed in section 2.4, namely NEW@105, (solid gray lines) for the eight rain
650 events of Table 1.

651 Figure 6: On the left panels, vertical profiles of Z obtained through the MRR new processing. On
652 the right panels, time series of the reflectivity: black solid lines are for the 2DVD, grey solid lines
653 represent Z computed from the RSDs obtained at 105 m through the MRR new processing
654 described in 2.4, and finally grey dashed lines are Z at 105 m provided by Metek in the "Averaged
655 data" files. (a, b) 1745-1900 UTC of 15 October 2012, (c ,d) 1300-1730 UTC of 31 October 2012.
656 In the colorbar the white color represents no data. Note the different time scales used for the two
657 events.

658 Figure 7: Box plot of *Z* at the different heights on 15 October 2012 during stratiform rain (a), and
659 convective rain (b). Note that *Z* was computed from the RSDs obtained through the application of
660 the MRR new processing presented in section 2.4. The solid vertical lines are the mean values of
661 vertical profile of *Z*.

662 Figure 8: As Figure 7 but for *D0*.

663 Figure 9: Vertical profile of RSD averaged over the stratiform minutes (a) and convective minutes
664 (b) of 15 October 2012.

665 **Tables**

666

Table 1: Summary of 2DVD and MRR recordings during HyMeX SOP 1 in Rome.

Day	Rainy Minutes	R_{cum_2DVD}	$R_{cum\_AVE@105}$	max (R_{2DVD})	max ($R_{AVE@105}$)	D_{max}	% of filtered drops
0913	313	19.56	9.18	49.99	23.3	6.21	13.2
0914	401	11.10	6.96	11.15	6.96	5.35	9.5
0930	435	16.02	10.05	88.18	98.02	6.15	13.3
1012	252	37.98	17.49	154.23	50.35	7.79	18.4
1015	189	25.33	14.82	114.34	110.33	7.49	19.5
1026	245	14.85	10.77	39.23	33.06	5.02	15.6
1031	916	37.64	28.05	56.89	43.31	6.18	15.6
1111	331	11.11	8.95	35.09	52.11	6.69	13.2

667
668

669
670
671
672
673

Table 2: Values of normalized standard error (NSE; dimensionless), normalized bias (NB; dimensionless and in dB in brackets), and correlation coefficient (cc; dimensionless) between *i)* the reflectivity factor computed from the data recorded by the 2DVD and that provided by the MRR standard processing ("*Averaged data*") at 105 m (AVE@105), and *ii)* the reflectivity factor computed from the data recorded by the 2DVD and the reflectivity computed from the RSD at 105 m obtained after the application of the new processing of the MRR raw spectra (NEW@105) (see section 2.4). For each day, second and third columns reports results percentage of minutes classified as convective and stratiform, respectively.

674

	C/S classification		Z_{2DVD} vs $Z_{AVE@105m}$			Z_{2DVD} vs $Z_{NEW@105m}$		
Day	% of convective minutes	% of stratiform minutes	NSE	NB (NB [dB])	cc	NSE	NB (NB [dB])	cc
0913	9	89	2.35	-0.57(-3.70)	0.867	0.72	-0.05(-0.21)	0.977
0914	0	98	1.05	-0.39(-2.12)	0.901	0.60	0.17(0.70)	0.958
0930	6	90	3.95	-0.57(-3.67)	0.630	1.19	-0.06(-0.26)	0.974
1012	22	74	3.53	-0.73(-5.68)	0.643	2.52	-0.32(-1.71)	0.845
1015	13	86	2.71	-0.78(-6.59)	0.829	2.13	-0.17(-0.81)	0.810
1026	3	93	1.70	-0.50(-3.06)	0.422	0.57	-0.04(-0.16)	0.946
1031	2	96	4.00	-0.47(-2.78)	0.475	4.56	0.23(0.90)	0.656
1111	7	92	2.59	-0.49(-2.98)	0.633	0.81	0.04(0.17)	0.965

675
676
677
678
679

680 **Figures**

681

682

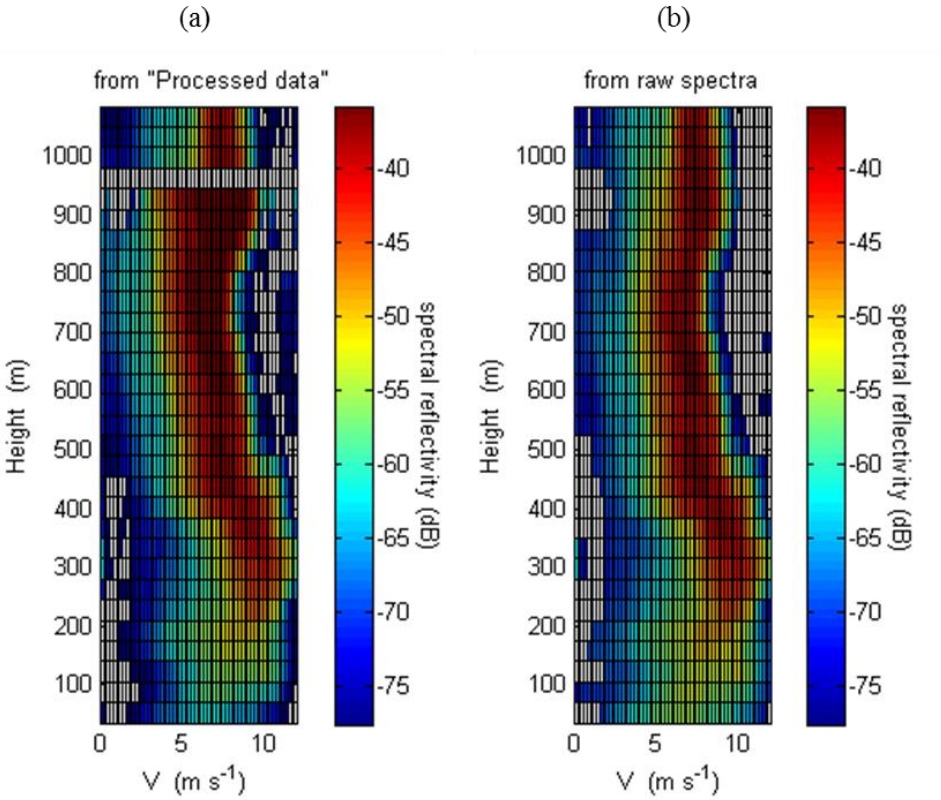

683

Figure 1: Reflectivity spectra provided by Metek in "*Processed data*" file on 15 October 2012 at 18:01:27 UTC (a) and reflectivity spectra obtained applying the noise removal procedure proposed by Maahn and Kollias (2012) to the raw spectra (b).

684

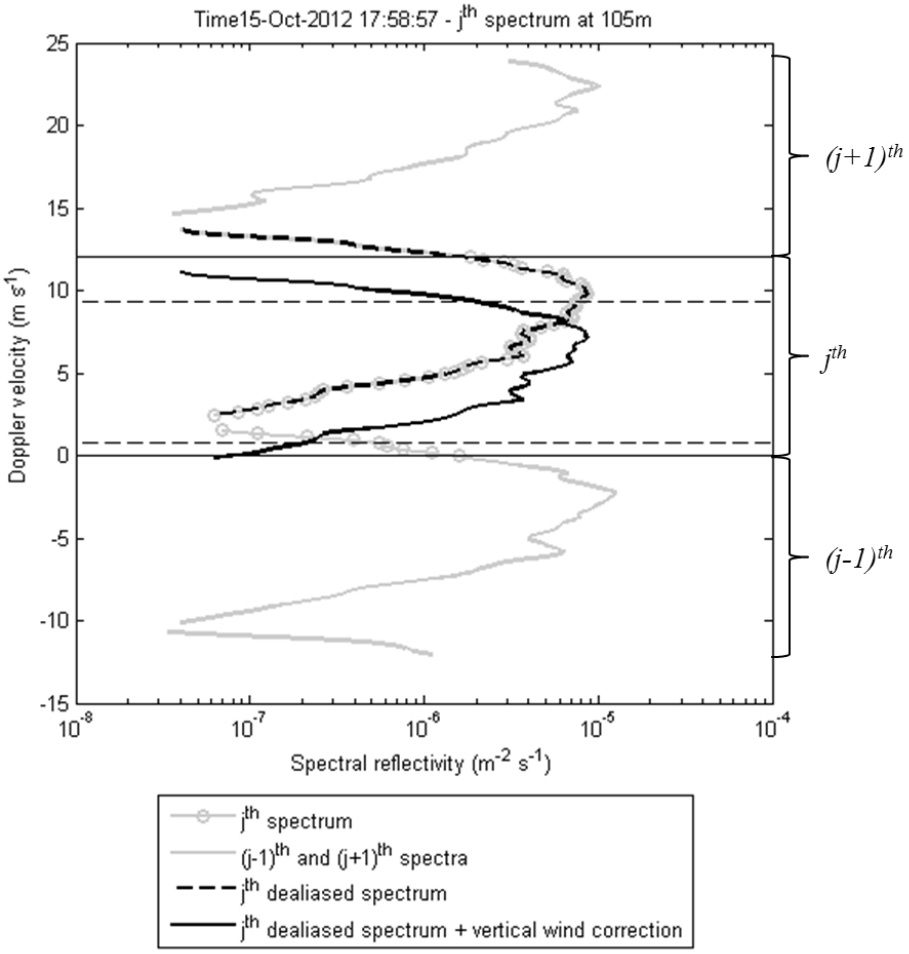

Figure 2: Example of the effects of the dealiasing and the correction for the presence of the vertical wind. The spectrum at 105 m at 17:58:57 UTC of 12 October 2012 is plotted with solid grey lines and circles and represents the *j*-th to be corrected. For the dealiasing procedure the (*j*-1)-th (namely at 70 m) and (*j*+1)-th (namely at 140 m) are considered (solid grey lines) and as result of this step, the dealiased spectrum is obtained and plotted with dashed black line. Finally, the solid black line is the dealiased spectra after the shift due to the presence of the vertical wind. The solid horizontal lines represent the Nyquist velocity boundaries (0 and +12 ms^{-1}), namely the limits of the j^{th} spectrum, while the dashed horizontal lines are the velocity range for the RSD retrieval, namely v = 0.76 ms^{-1} and v = 9.36 ms^{-1}.

685

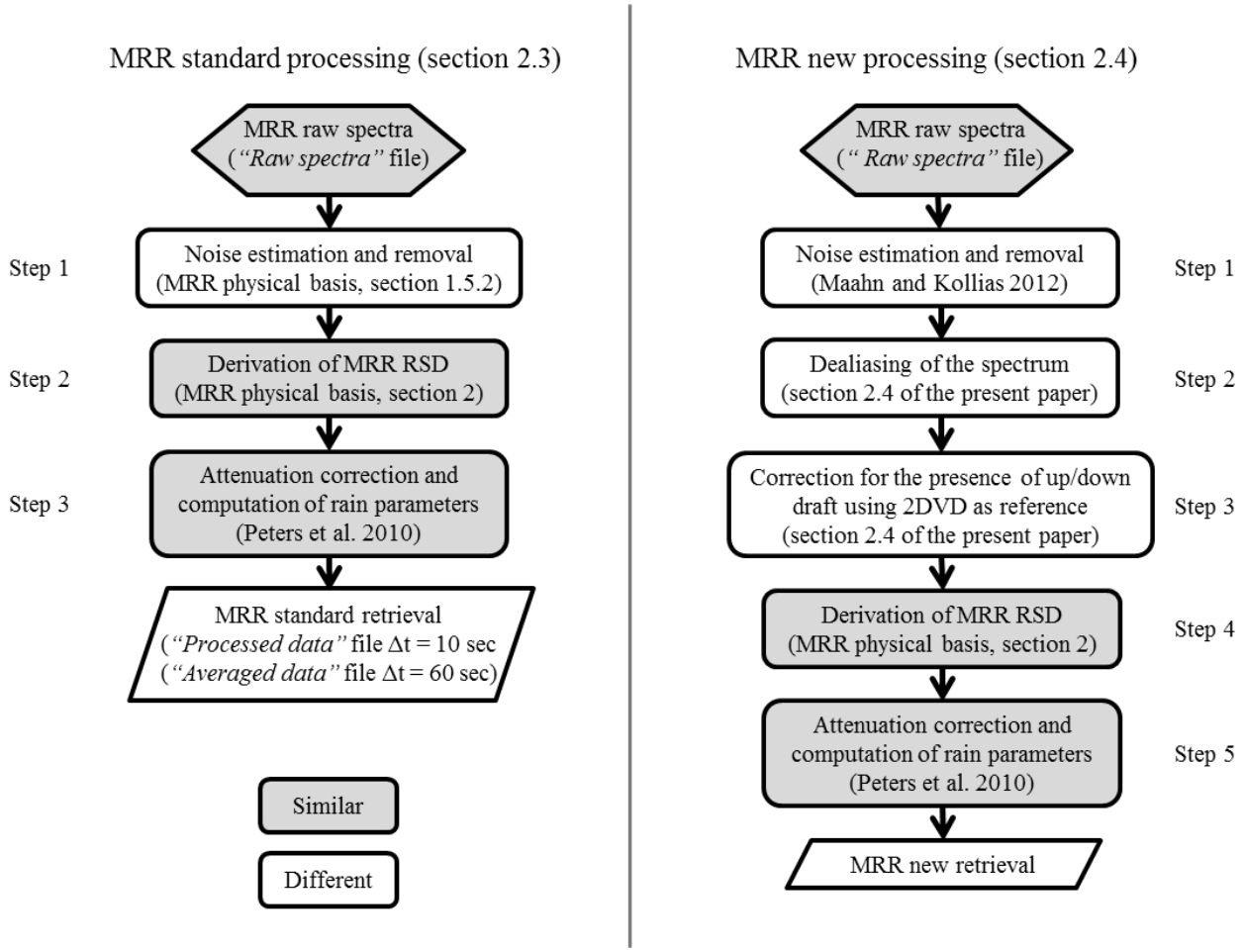

Figure 3: Flowchart of the processing steps involved in the MRR standard processing (on the left) and the MRR new processing (on the right).

686

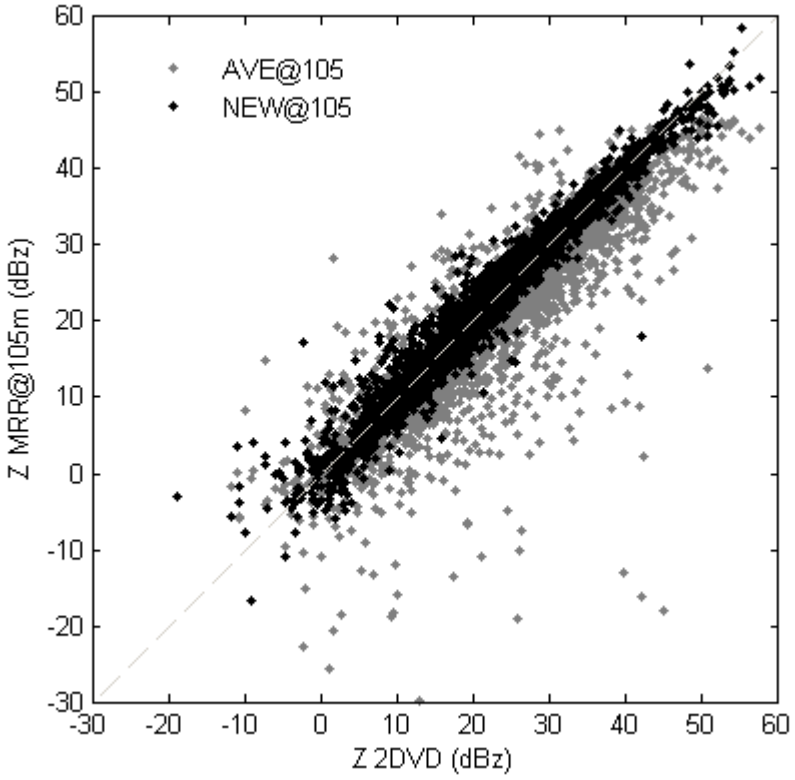

687

Figure 4: Scatterplot comparing reflectivity factor from 2DVD spectra with *i)* reflectivity factor of MRR standard product at 105 m, namely AVE@105, (grey dots), and *ii)* reflectivity factor of MRR using the processing approach proposed in this study, namely NEW@105, (black dots).

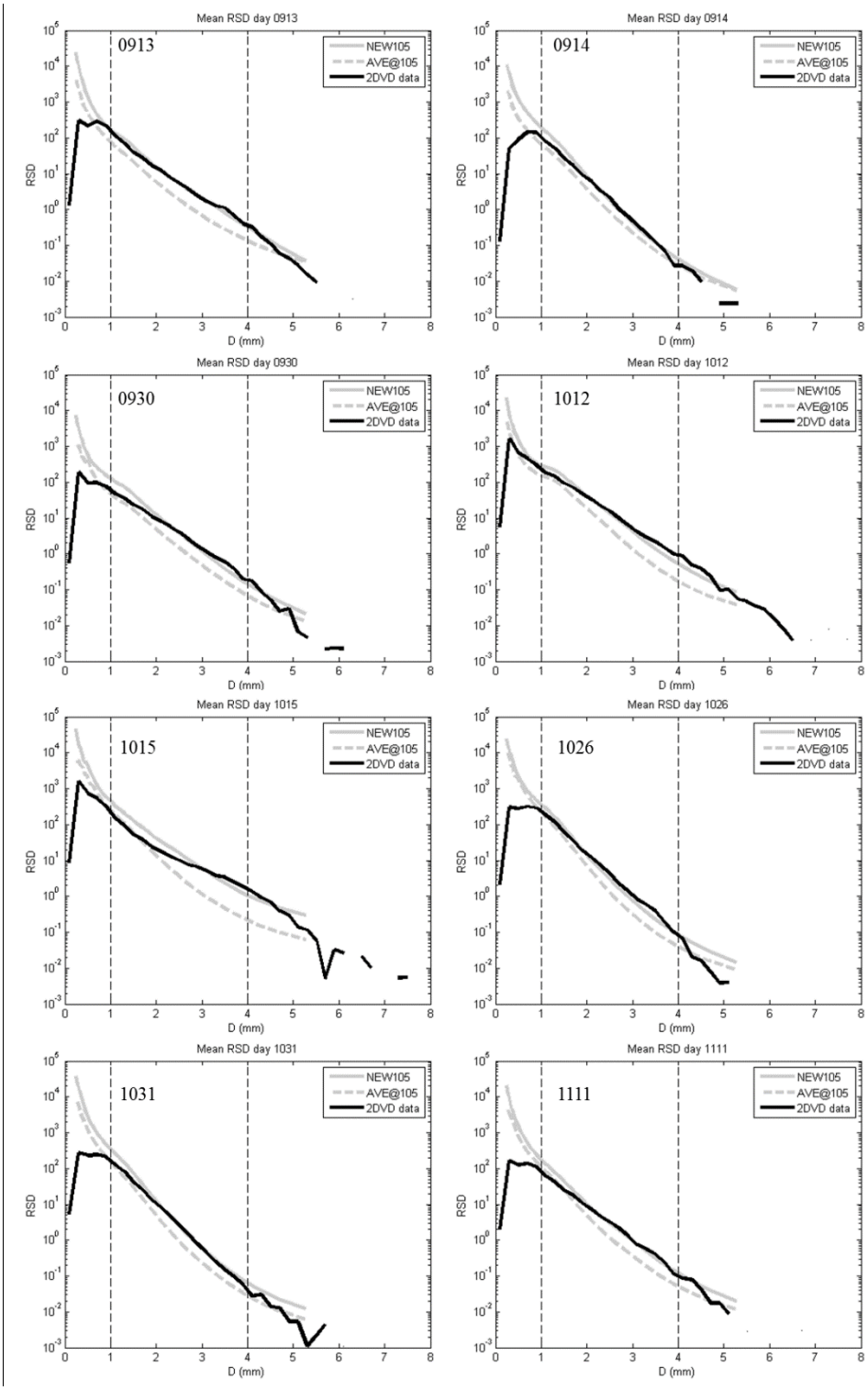

Figure 5: Averaged RSD obtained from 2DVD data (black solid lines), MRR "*Averaged data*" at 105 m, namely AVE@105, (dashed grey lines), and MRR raw spectra reprocessed following the new procedure proposed in section 2.4, namely NEW@105, (solid gray lines) for the eight rain events of Table 1. The black dashed lines represent at D = 1 mm and D = 4 mm help the classification of the spectrum (namely small drops for D < 1 mm, midsize drops for 1 mm < D < 4 mm, and large drops for D > 4 mm).

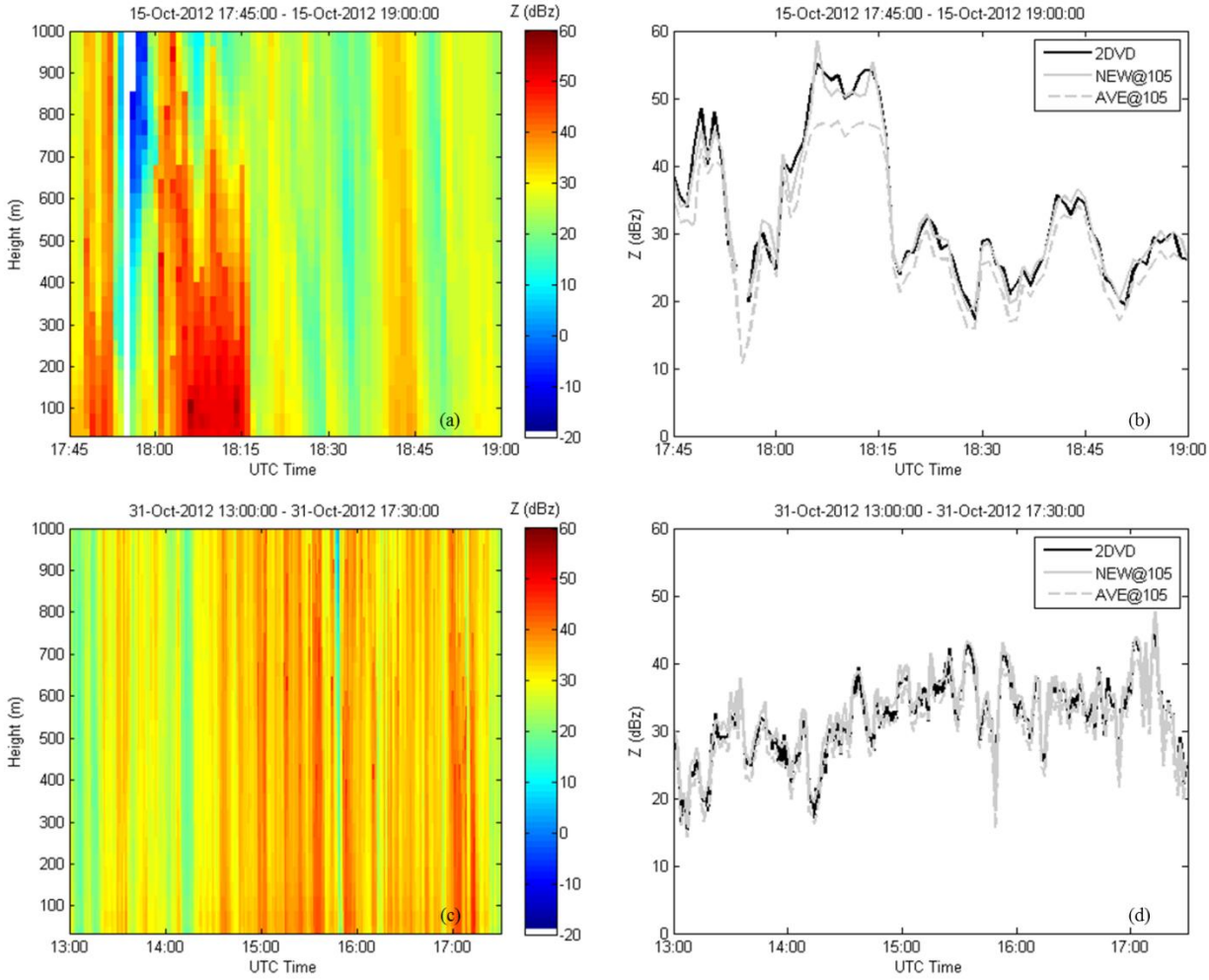

Figure 6: On the left panels, vertical profiles of Z obtained through the MRR new processing. On the right panels, time series of the reflectivity: black solid lines are for the 2DVD, grey solid lines represent *Z* computed from the RSDs obtained at 105 m through the MRR new processing described in 2.4, and finally grey dashed lines are *Z* at 105 m provided by Metek in the "*Averaged data*" files. (a, b) 1745-1900 UTC of 15 October 2012, (c ,d) 1300-1730 UTC of 31 October 2012. In the colorbar the white color represents no data. Note the different time scales used for the two events.

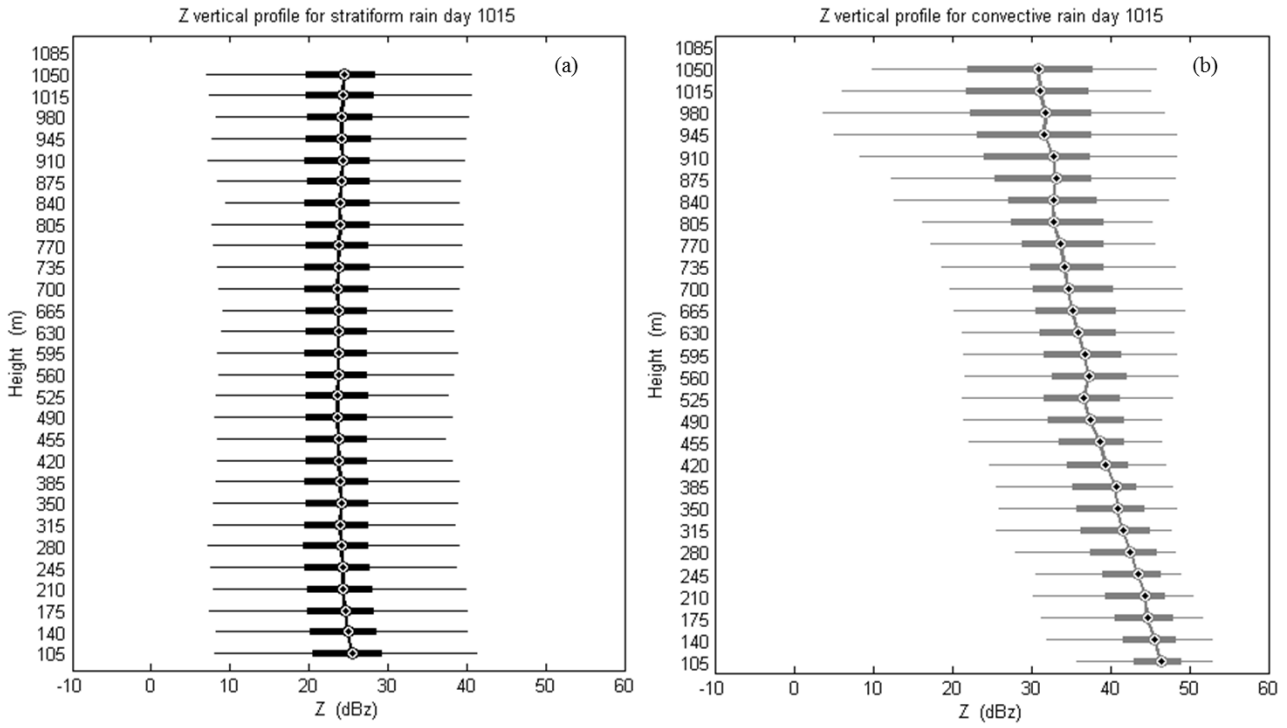

Figure 7: Box plot of *Z* at the different heights on 15 October 2012 during stratiform rain (a), and convective rain (b). Note that *Z* was computed from the RSDs obtained through the application of the MRR new processing presented in section 2.4. The solid vertical lines are the mean values of vertical profile of *Z*.

690

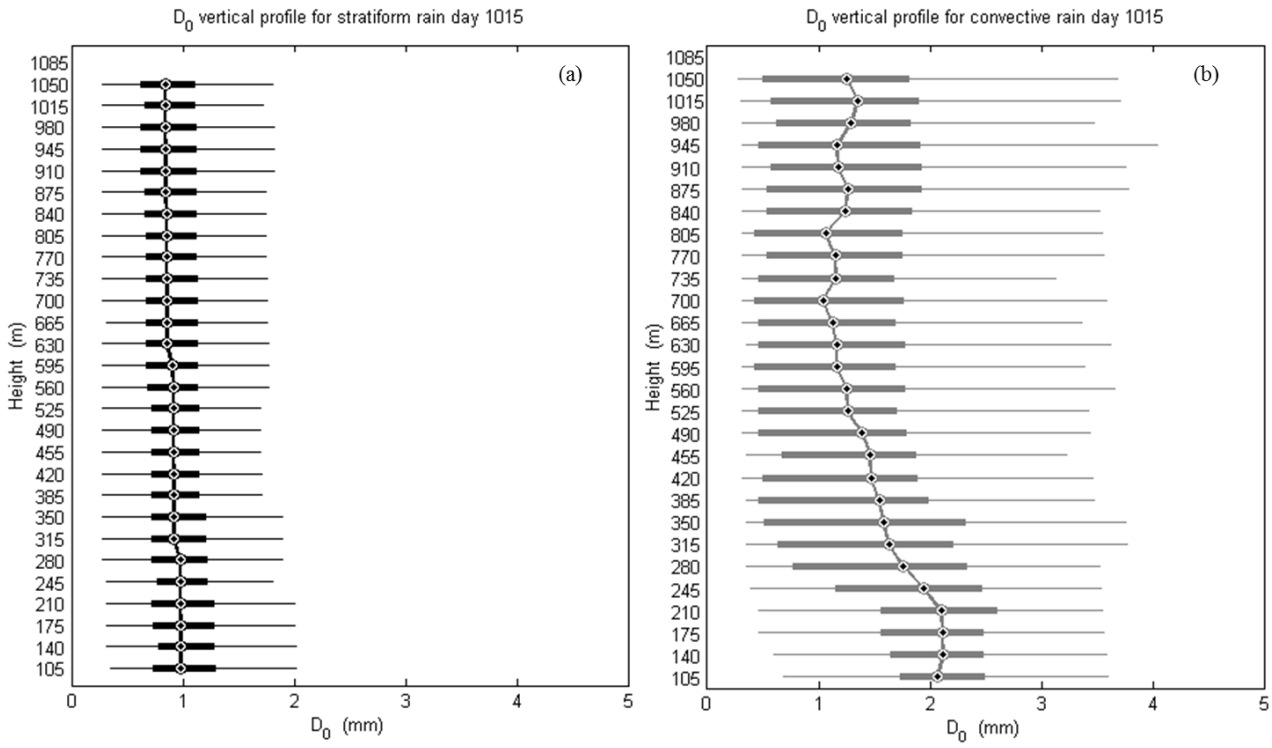

Figure 8: As Figure 7 but for D_0.

691

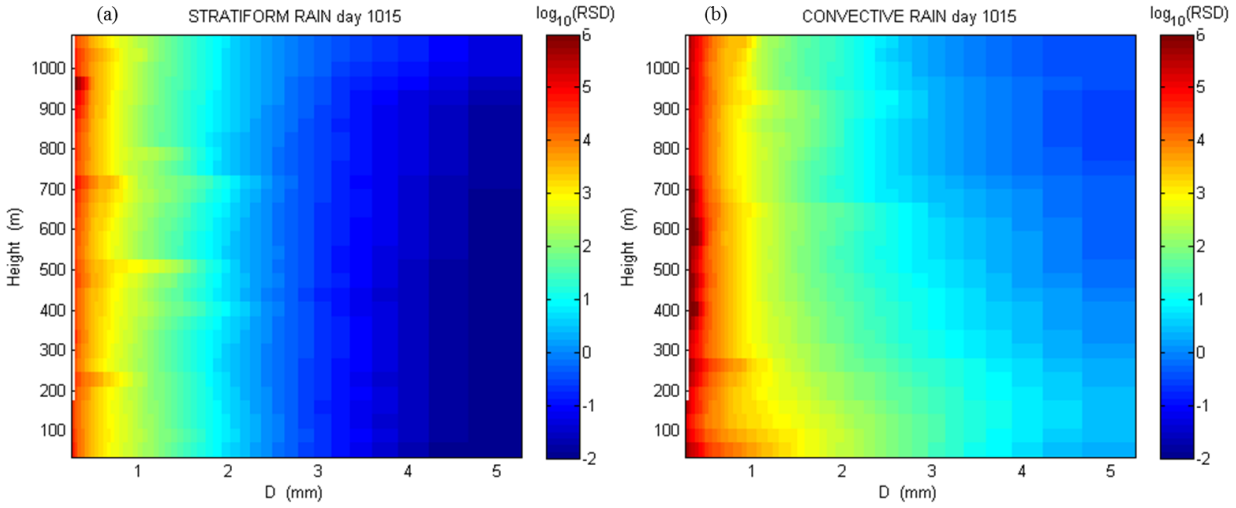

692

Figure 9: Vertical profile of RSD averaged over the stratiform minutes (a) and convective minutes (b) of 15 October 2012.

693